

Never too Cocky to Cooperate: An FIM and RL-based USV-AUV Collaborative System for Underwater Tasks in Extreme Sea Conditions

Jingzehua Xu¹, Guanwen Xie¹, Jiwei Tang², Yimian Ding¹, Weiyi Liu¹, Junhao Huang³, Shuai Zhang⁴ and Yi Li¹

Abstract—This paper develops a novel unmanned surface vehicle (USV)–autonomous underwater vehicle (AUV) collaborative system designed to enhance underwater task performance in extreme sea conditions. The system integrates a dual strategy: (1) high-precision multi-AUV localization enabled by Fisher information matrix-optimized USV path planning, and (2) reinforcement learning-based cooperative planning and control method for multi-AUV task execution. Extensive experimental evaluations in the underwater data collection task demonstrate the system’s operational feasibility, with quantitative results showing significant performance improvements over baseline methods. The proposed system exhibits robust coordination capabilities between USV and AUVs while maintaining stability in extreme sea conditions. To facilitate reproducibility and community advancement, we provide an open-source simulation toolkit available at: <https://github.com/360ZMEM/USV-AUV-colab>.

I. INTRODUCTION

Autonomous underwater vehicles (AUVs) have become indispensable tools for underwater exploration, enabling critical tasks such as environmental monitoring [1], seabed mapping [2], and biological research [3]. However, traditional approaches relying on single-AUV systems or loosely coordinated swarms face significant limitations in positioning accuracy, scalability, and energy efficiency [4], particularly in extreme sea conditions where dynamic currents and turbulence exacerbate these challenges [5].

A central bottleneck lies in AUV localization: conventional methods like inertial navigation systems (INS) and standalone acoustic beacons suffer from error accumulation and signal degradation in dynamic environments, leading to unreliable positioning over prolonged missions [6]. To address this, integrating AUVs with an unmanned surface vehicle (USV) as a mobile base station offers a promising solution [7]. The USV provides real-time, high-precision

This article has been presented in part at the IEEE International Conference on Acoustics, Speech and Signal Processing (ICASSP), Hyderabad, India, in April 2025.

¹J. Xu, G. Xie, Y. Ding, W. Liu and Y. Li are with Tsinghua Shenzhen International Graduate School, Tsinghua University, Shenzhen, 518055, China. E-mail: {xjzh23, xgw24, dingym24, liuw24}@mails.tsinghua.edu.cn, liyi@sz.tsinghua.edu.cn.

²J. Tang is with Department of Data and Systems Engineering, The University of Hong Kong, Pokfulam, Hong Kong. E-mail: tangjiwei7@gmail.com.

³J. Tang is with School of Engineering Science, University of Chinese Academy of Sciences, Beijing, China, E-mail: huangjunhao22@mailsucas.ac.cn.

⁴S. Zhang is with Department of Data Science, New Jersey Institute of Technology, NJ 07102, USA. E-mail: sz457@njit.edu.

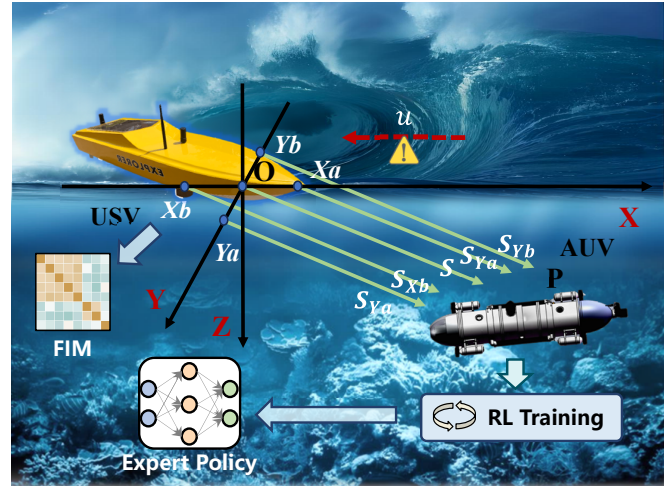


Fig. 1. The proposed USV-AUV collaborative system is designed to perform underwater tasks efficiently. It employs a dual-strategy approach, combining FIM-based USV path planning for precise AUV positioning and RL-based training to enhance adaptive decision-making in AUVs. This integrated system ensures effective cooperation between USV and AUVs, optimizing mission performance in extreme sea conditions.

positioning by acting as a communication and navigation hub, delivering GPS-corrected acoustic updates to submerged AUVs [8]. This synergy not only mitigates error drift but also enhances multi-AUV coordination [9], making USV-AUV collaboration a growing research focus.

Despite recent advances, existing USV-AUV frameworks often lack the intelligence and adaptability required for complex tasks in extreme sea conditions [10]. For instance, while Ultra-Short Baseline (USBL) positioning via USV improves localization, most approaches either fix the USV at static coordinates or employ heuristic path planning [11]. Such rigidity results in inefficient USV-AUV linkage and fails to adapt to dynamic ocean environments, leading to suboptimal positioning and task performance. Further, traditional AUV control strategies (e.g., PID, fuzzy control) rely heavily on precise dynamic models, exhibit poor adaptability to turbulence, and struggle with multi-objective optimization or high-dimensional sensor data [12]. Crucially, many studies treat ocean dynamics as negligible noise—an unrealistic assumption in extreme conditions [13].

To address these challenges, a dual strategy is essential: adaptive planning and control policy to enable dynamic decision-making in uncertain environments without relying

on rigid models, while optimizing multi-AUV collaboration for efficient task execution, and uncertainty and information-aware path planning method to improve the accuracy of AUV positioning via USV to enhance the robustness of the USV-AUV system, mitigating localization errors caused by extreme sea conditions.

This motivates the integration of reinforcement learning (RL) and Fisher Information Matrix (FIM) optimization—a synergistic approach that jointly tackles control and localization challenges [14]. On one hand, RL’s model-free adaptive optimization enables AUVs to learn robust policies through environmental interaction, overcoming nonlinearities and time-varying disturbances without precise dynamic models [15], [16]. Multi-Agent RL (MARL) further enhances cooperative planning and control, enabling efficient multi-AUV coordination under communication constraints [17]. On the other hand, FIM-based optimization directly quantifies and minimizes positioning uncertainty via USV path planning for maximizing the system’s information content, thereby reducing the Cramér-Rao Bound (CRB) for AUV navigation [14]. By combining RL’s adaptability with FIM’s precision, the proposed system achieves both intelligent decision-making and high-accuracy localization—a critical requirement for extreme sea scenarios.

Based on above analysis, this paper develops a FIM and RL-based USV-AUV collaborative system for underwater tasks in extreme sea conditions to improve the mission complete efficiency, and contributions are listed as follows:

- A novel USV-AUV collaborative system is developed, which integrates a FIM and RL-based dual strategy to enable dynamic decision-making and uncertainty and information-aware capability to improve the mission complete efficiency for underwater tasks.
- This system realizes accurate positioning of AUVs via USV path planning through minimizing the determinant of the system’s FIM. Based on this, through integrating environment-aware ability into state space, and shaped reward function for multi-AUV collaboration, we further use RL to empower multi-AUV with intelligence and the adaptability to the underwater task.
- Through comprehensive experiments in the underwater data collection task, our system showcases superior feasibility and excellent performance with robustness in extreme sea conditions.

The remainder of this paper is organized as follows: Section II reviews related work on USV-AUV collaboration in underwater tasks. Section III details the methodology of this work. Section IV describes the environmental simulations and experimental results. Finally, Section V concludes the paper and outlines future directions.

II. RELATED WORK

A. Advances in USV-AUV Collaborative Systems

The USV-AUV collaborative system has garnered significant attention due to its potential in marine exploration

and environmental monitoring. Early research primarily addressed communication and coordination challenges, including acoustic communication modems and surface relay systems [18], as well as task allocation mechanisms where USVs serve as mobile base stations [19]. Concurrently, cooperative navigation frameworks developed for GPS-denied environments significantly enhanced AUV positioning capabilities [20].

Recent studies have focused on multi-agent autonomous collaboration, with machine learning algorithms enabling cooperative tasks such as seabed mapping [21]. Hybrid communication systems combining acoustic and radio links have improved system reliability [22]. Although challenges in real-time decision-making under environmental uncertainties persist, emerging technologies such as swarm intelligence and RL offer solutions for scalable collaboration [23].

B. FIM-based Approaches for USV

For USVs operating in dynamic marine environments, FIM has been applied to adaptive sampling strategies, where vehicle trajectories are optimized to improve environmental field reconstruction (e.g., salinity or temperature mapping) [24]. These approaches often combine FIM metrics with gradient-based or sampling-based planners to balance exploration efficiency with motion constraints [25].

Recent advances have focused on integrating FIM into real-time USV path planning under environmental disturbances and communication constraints. Cooperative scenarios, where USV and multiple AUVs collaboratively maximize joint FIM determinant, have also been explored using distributed optimization techniques [14]. Challenges persist in computational scalability for high-dimensional FIM calculations and in robustifying FIM metrics against sensor noise and model mismatches. Emerging solutions include Gaussian process-based approximations of FIM [26] and hybrid learning-control architectures that adaptively tune information-driven objectives [27].

C. RL-based AUV Control and Planning

Reinforcement learning (RL) has become a prominent approach for AUV control and planning in complex marine environments. Early studies employed value-based methods like Q-learning for basic navigation tasks [28], while later work adopted policy gradient methods to handle dynamic currents [29]. The introduction of deep RL enabled end-to-end learning from sensor data [30], though these methods faced challenges in partial observability and data efficiency.

Recent advances focus on multi-agent systems and hybrid approaches. Cooperative RL allows AUV teams to collaboratively perform tasks [31], while model-based RL improves sample efficiency using oceanographic models [32]. Current research addresses communication constraints and safety guarantees through hierarchical RL and meta-learning [33], though real-world deployment challenges remain.

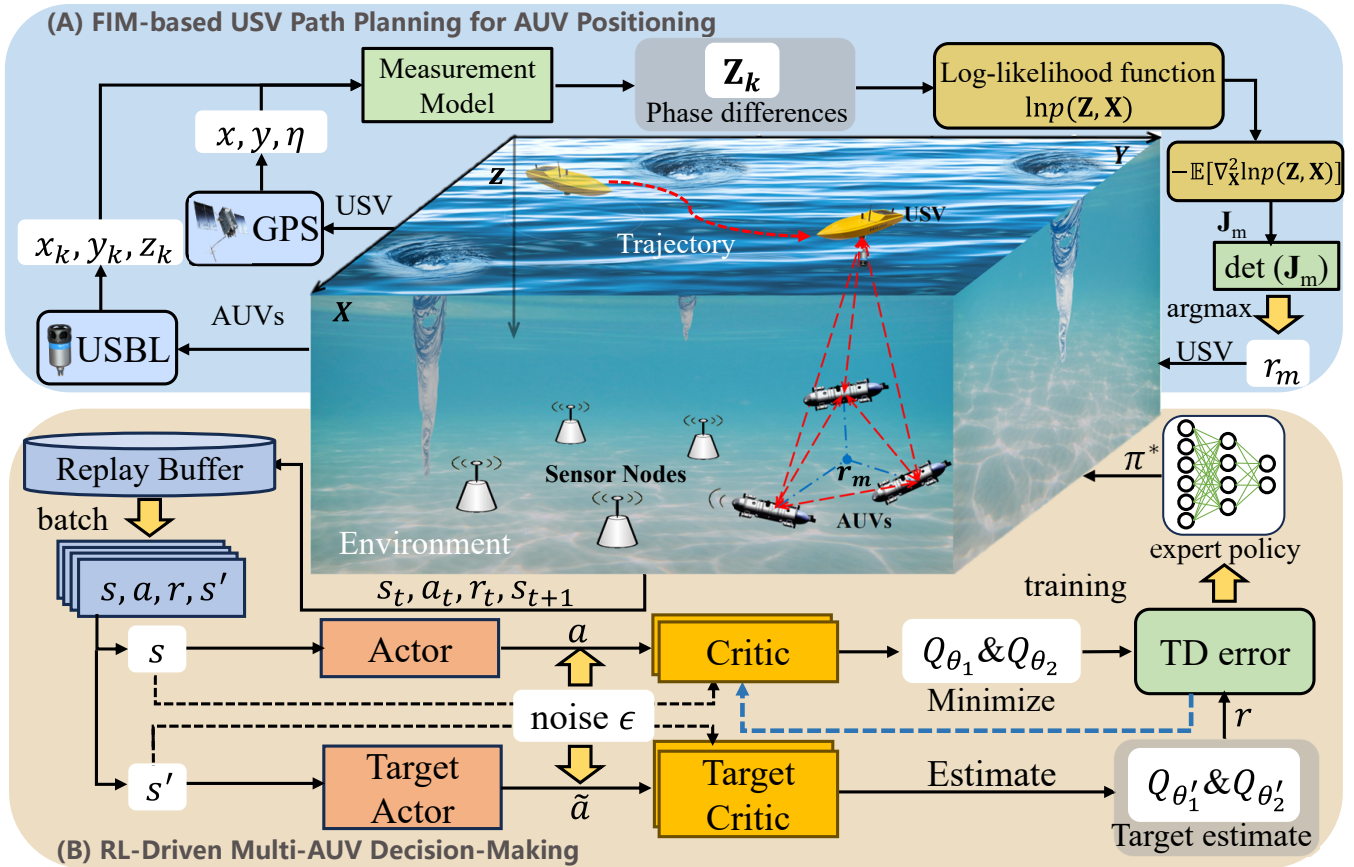


Fig. 2. **The overall architecture of proposed USV-AUV collaborative system**, which integrates FIM optimization and RL to enhance adaptability and precision in dynamic marine environments. Through optimization of FIM’s determinant, USV can realize path planning to improve AUV positioning accuracy. Besides, TD3 algorithm enables multi-AUV systems to learn efficient navigation and collaboration strategies through iterations of RL training. Together, they ensure robust performance despite disturbances like tides or turbulence, continuously refining behavior through real-time feedback in the extreme sea conditions.

III. METHODOLOGY

A. System Architecture

The proposed USV-AUV collaborative system architecture combines FIM optimization and RL training to achieve dynamic decision-making, uncertainty-aware capabilities, and adaptive behavior in challenging marine environments. As illustrated in Fig. 2, the system adopts a dual-strategy framework: FIM optimizes AUV positioning accuracy through USV path planning, while RL enhances multi-AUV intelligence and adaptability to dynamic ocean conditions.

Specifically, the system employs FIM to maximize AUV localization precision by minimizing the determinant of the FIM, thereby reducing estimation uncertainty in the underwater environment. The USV dynamically adjusts its path planning based on real-time FIM calculations, ensuring optimal positioning support for the AUVs. This mathematical approach enhances system robustness, even when external disturbances—such as tidal waves or turbulence—degrade sensor measurements.

To further improve adaptability, the system integrates an RL framework where the state space incorporates environment-aware data, and the reward function evaluates USV-AUV collaboration efficiency. This enables multi-AUV

systems to learn and refine navigation and task execution strategies under extreme conditions, increasing mission complete efficiency. By continuously adapting to real-time environmental feedback, the RL component ensures sustained performance optimization.

B. FIM-based USV Path Planning for AUV Positioning

Our system enables accurate underwater vehicle positioning through an optimized USV navigation strategy, leveraging USBL technology, while further using the optimization of FIM’s determinant to realize efficient USV path planning to minimize AUV positioning error. As shown in Fig. 1 and Fig. 2, the system architecture consists of:

- A surface USV located at coordinates (x, y, η) equipped with a USBL transducer array (inter-element spacing $d/2$), while using GPS for self-positioning.
- Multiple AUVs deployed at underwater positions $(x_k, y_k, z_k), k = 1, 2, \dots, m$.

The positioning framework is built upon a measurement model in USBL that correlates observed phase differences with AUV locations. This relationship is mathematically expressed as [34]:

$$\mathbf{Z}_k = \mathbf{h}_k(\mathbf{X}) + \mathbf{u}_k, \quad \mathbf{X} = [x, y]^\top, \quad (1)$$

where $\mathbf{h}_k = [\Delta\varphi_{x,k}, \Delta\varphi_{y,k}]^\top$ is the phase differences vector, whose elements can be expressed as:

$$\Delta\varphi_{x,k} = \frac{2\pi f d(x_k - x)}{cS_k}, \quad (2)$$

$$\Delta\varphi_{y,k} = \frac{2\pi f d(y_k - y)}{cS_k}, \quad (3)$$

where c represents the speed of sound and f indicates the signal frequency. Additionally,

$S_k = \sqrt{(x_k - x)^2 + (y_k - y)^2 + z_k^2}$ is the slant range,

$\mathbf{u}_k \sim \mathcal{N}(0, \sigma^2 \mathbf{I})$ represents measurement noise.

To rigorously evaluate the system's localization accuracy, we derive the FIM from this measurement model. The FIM provides a quantitative measure of position estimation precision by analyzing the information content in the USBL phase difference measurements.

The FIM is derived by calculating the expectation of the second partial derivatives of the log-likelihood function. This quantifies how much information the measurements carry about the unknown USV position \mathbf{X} : Under the assumption that $\mathbb{E}[\mathbf{Z}_k - \mathbf{h}_k(\mathbf{X})] = 0$, the FIM is expressed as [35]:

$$\mathbf{J}_m = -\mathbb{E}[\nabla_{\mathbf{X}}^2 \ln p(\mathbf{Z}, \mathbf{X})], \quad (4)$$

$$\ln p(\mathbf{Z}, \mathbf{X}) = -\frac{1}{2} \sum_{k=1}^m [\mathbf{Z}_k - \mathbf{h}_k(\mathbf{X})]^\top \mathbf{R}^{-1} [\mathbf{Z}_k - \mathbf{h}_k(\mathbf{X})] + C, \quad (5)$$

where $\mathbf{R} = \sigma^2 \mathbf{I}$ denotes the measurement noise covariance matrix, and C is the constant related to \mathbf{R} .

The determinant of \mathbf{J}_m serves as a scalar metric for overall positioning accuracy. By simplifying $\det(\mathbf{J}_m)$. For geometric interpretation and optimization, we isolate two critical geometric factors:

$$\det(\mathbf{J}_m) \propto \underbrace{\left(\sum_{k=1}^m \frac{1}{S_k^2} \sum_{k=1}^m \frac{\sin^4 \gamma_k}{S_k^2} \right)^2}_{\text{Depth and Slant Factor}} + \underbrace{\sum_{1 \leq i < j \leq m} A_i A_j \sin^2(\varphi_i - \varphi_j)}_{\text{Angular Diversity}}, \quad (6)$$

where $A_k = \frac{p_k^4 - 2S_k^2 p_k^2}{2S_k^6}$, with $p_k^2 = x_k^2 + y_k^2$, while $\sin \gamma_k = \frac{z_k}{S_k}$, and $\varphi_k = \arctan(y_k/x_k)$ denotes the azimuth angle. The first term emphasizes depth and slant-dependent observability, while the second term penalizes collinear AUV placements. This directly motivates the optimal formations, which reveals that optimal positioning requires:

- 1) Minimizing slant ranges S_k to AUVs.
- 2) Maximizing angular separation between AUV projections through $\sin^2(\varphi_i - \varphi_j)$ terms.
- 3) Balancing depth-to-range ratios through $\sin^4 \gamma_k$ terms.

For the convenience of research without loss of generality, this work only considers the influence of different angles between AUVs of underwater targets on positioning accuracy. When the distance between the AUVs and the USV is equal and the AUVs are at the same depth, only the angle of the

Algorithm 1 RL Training using TD3

- 1: Initialize policy π_ϕ and critics $Q_{\theta_1}, Q_{\theta_2}$
 - 2: Initialize target networks $\phi' \leftarrow \phi, \theta'_i \leftarrow \theta_i$
 - 3: Initialize replay buffer \mathcal{D}
 - 4: **for** each episode **do**
 - 5: Observe initial state s_0
 - 6: **for** each timestep **do**
 - 7: Sample action $a_t = \pi_\phi(s_t) + \epsilon, \epsilon \sim \mathcal{N}(0, \sigma)$
 - 8: Execute a_t , observe s_{t+1} and r_t
 - 9: Store (s_t, a_t, r_t, s_{t+1}) in \mathcal{D}
 - 10: **if** update time **then**
 - 11: Sample batch $(s, a, r, s') \sim \mathcal{D}$
 - 12: Compute target actions $\tilde{a} = \pi_{\phi'}(s') + \text{clip}(\epsilon, -c, c)$
 - 13: Update critics using $y = r + \gamma \min_{i=1,2} Q_{\theta'_i}(s', \tilde{a})$
 - 14: **if** actor update delay **then**
 - 15: Calculate policy gradient:

$$\nabla_{\phi} J(\phi) = \mathbb{E}[\nabla_a Q_{\theta_1}(s, a)|_{a=\pi_\phi(s)} \nabla_{\phi} \pi_\phi(s)]$$
 - 16: Q-networks update:

$$\theta_i \leftarrow \theta_i - \lambda_Q \nabla_{\theta_i} \mathbb{E}[(Q_{\theta_i}(s, a) - y)^2]$$
 - 17: Delayed policy update:

$$\phi \leftarrow \phi + \lambda_\pi \nabla_{\phi} J(\phi)$$
 - 18: Target network updates:

$$\theta'_i \leftarrow \tau \theta_i + (1 - \tau) \theta'_i$$

$$\phi' \leftarrow \tau \phi + (1 - \tau) \phi'$$
 - 19: **end if**
 - 20: **end if**
 - 21: **end if**
 - 22: **end for**
 - 23: **end if**
 - 24: **end if**
 - 25: **end for**
 - 26: **end for**
-

AUVs is considered, and the influence of AUV formation on positioning accuracy is only related to $\sin^2 \alpha_{ij}$:

$$\det(\mathbf{J}_m) = \left(\frac{4\pi^2 f^2 d^2}{\sigma^2 c^2} \right)^2 \left[3m \frac{\sin^2 \gamma_0}{S_0^4} + \frac{(\sin^4 \gamma_0 + 1)^2}{S_0^4} \chi \right], \quad (7)$$

where $\sin \gamma_0 = \frac{z_0}{S_0}$, while $\chi = \sum_{1 \leq i < j \leq m} \sin^2 \alpha_{ij}$, with $\alpha_{ij} = \varphi_i - \varphi_j$ representing the angle between the projections of two AUVs and USV.

As illustrated in Fig. 2, by maximizing the determinant $\det(\mathbf{J}_m)$, we can determine the optimal horizontal distance r_m between the USV and multiple AUVs:

$$r_m = \operatorname{argmax} \{ \det(\mathbf{J}_m) \}. \quad (8)$$

Through calculating the waypoints using Eq. (8) with the maximum $\det(\mathbf{J}_m)$, we can implement USV path planning to minimize AUV positioning errors through above process.

C. RL-Driven Multi-AUV Decision-Making

Our approach leverages the Twin Delayed Deep Deterministic Policy Gradient (TD3) algorithm, which extends the Deep Deterministic Policy Gradient (DDPG) algorithm with three key improvements: (1) clipped double Q-learning

to mitigate overestimation bias, (2) delayed policy updates to stabilize training, and (3) target policy smoothing to prevent overfitting to narrow peaks in the value function [36]. These characteristics make TD3 particularly suitable for underwater vehicle control, where precise continuous actions are required and the dynamics are highly coupled across degrees of freedom.

In continuous control tasks, we model the environment as a Markov Decision Process (MDP) for further RL training with:

$$\langle \mathcal{S}, \mathcal{A}, \mathcal{R}, \mathcal{P}(\cdot|s, a), \gamma \rangle, \quad (9)$$

where continuous state space \mathcal{S} , continuous action space \mathcal{A} , reward function $r : \mathcal{S} \times \mathcal{A} \rightarrow \mathbb{R}$. $\mathcal{P}(\cdot|s, a) \sim (0, 1)$ is the state transition probability. $\gamma \in [0, 1]$ represents the discount factor.

Given state space \mathcal{S} and action space \mathcal{A} , our objective in the underwater tasks is to obtain the expert policy through maximizing discounted cumulative reward:

$$\pi^* = \operatorname{argmax}\{J(\pi)\} = \operatorname{argmax}\{\mathbb{E}_\pi \left[\sum_{t=0}^{\infty} \gamma^t r(s_t, a_t) \right]\}, \quad (10)$$

where $\pi : \mathcal{S} \rightarrow \mathcal{A}$ is a deterministic policy. The agent's objective is to find the optimal policy π^* that maximizes the expected return: where $\gamma \in [0, 1]$ is the discount factor. This infinite-horizon formulation requires careful treatment of the value function approximation.

The action-value function $Q^\pi(s, a)$ represents the expected return when taking action a in state s and following policy π thereafter. It satisfies the fundamental Bellman equation:

$$Q^\pi(s, a) = \mathbb{E}_{s' \sim \mathcal{P}(\cdot|s, a)} [r(s, a) + \gamma Q^\pi(s', \pi(s'))]. \quad (11)$$

This recursive relationship forms the basis for temporal difference learning. However, when combined with function approximation and off-policy updates, it can lead to value overestimation.

To mitigate overestimation bias, TD3 maintains two separate Q-function approximators Q_{θ_1} and Q_{θ_2} with independent parameters.

The target noise ϵ serves as a regularizer, preventing the policy from exploiting overestimated Q-values. The clipped Gaussian noise ensures the perturbation stays within reasonable bounds:

$$\pi_{\text{target}}(s') = \pi_{\phi'}(s') + \operatorname{clip}(\epsilon, -c, c). \quad (12)$$

This smoothing can be interpreted as adding a small entropy term to the deterministic policy.

The target value computation uses the minimum of these two estimates: Maintain two Q-networks Q_{θ_1} and Q_{θ_2} with target networks:

$$y = r + \gamma \min_{i=1,2} Q_{\theta'_i}(s', \pi_{\phi'}(s') + \operatorname{clip}(\epsilon, -c, c)), \quad (13)$$

where $\epsilon \sim \operatorname{clip}(\mathcal{N}(0, \sigma), -c, c)$ adds noise to the target action for smoothing. This minimum operator provides a lower bound on the true value function, as we can show that:

$$\min_{i=1,2} Q_{\theta'_i}(s', a') \leq Q^\pi(s', a'), \quad (14)$$

for any (s', a') under mild assumptions about approximation errors.

Thus, we can obtain Critic's loss function is based on the TD error of the Bellman equation:

$$\mathcal{L}(\theta_i) = \mathbb{E}_{(s, a, r, s') \sim \mathcal{D}} [(Q_{\theta_i}(s, a) - y)^2], \quad i = 1, 2. \quad (15)$$

The policy network updates less frequently than the Q-functions (typically every $d = 2$ steps). This delay allows the value estimates to stabilize before the policy is adjusted, reducing error propagation. According to the deterministic policy gradient theorem

$$\nabla_\phi J(\phi) = \int_{\mathcal{S}} \rho^\pi(s) \nabla_a Q^\pi(s, a) \Big|_{a=\pi_\phi(s)} \nabla_\phi \pi_\phi(s) ds, \quad (16)$$

we can get the policy gradient, which is computed as:

$$\nabla_\phi J(\phi) = \mathbb{E}_{s \sim \mathcal{D}} \left[\nabla_a Q_{\theta_1}(s, a) \Big|_{a=\pi_\phi(s)} \nabla_\phi \pi_\phi(s) \right]. \quad (17)$$

Note that only Q_{θ_1} is used for the policy gradient to prevent the "chasing" behavior that could occur if both Q-networks were used simultaneously.

In practice, we can estimate the policy gradient using Monte Carlo method:

$$\nabla_\phi J(\phi) \approx \frac{1}{N} \sum_{i=1}^N \nabla_a Q(s_i, a) \Big|_{a=\pi_\phi(s_i)} \nabla_\phi \pi_\phi(s_i). \quad (18)$$

Finally, we update the policy network, and update the target networks using soft update strategy. The overall RL training using TD3 algorithm has been shown in pseudo-code Algorithm 1.

IV. EXPERIMENTS AND ANALYSIS

In this section, we verify the effectiveness of the proposed USV-AUV collaborative system in extreme sea conditions through comprehensive simulation experiments. Furthermore, we present the experimental results with further analysis and discussion.

A. Task Description and Experimental Settings

Given the limited availability of open-source underwater tasks, we selected the underwater data collection task as a benchmark scenario to validate our system. In this application scenario, multiple AUVs and a USV work collaboratively to collect data from sensor nodes (SNs) deployed in the Internet of Underwater Things (IoUT) environments, while simultaneously optimizing multiple objectives including seveded SN number (SSN) and sum data rate (SDR) maximization, collision avoidance, and energy consumption (EC) minimization. The specific parameter configurations employed in our study are comprehensively listed in Table 1. For further technical specifications and detailed task parameters, readers may consult our prior research work [5].

As for the RL algorithm, the TD3 implementation uses separate networks for the actor (policy) and critics (Q-functions):

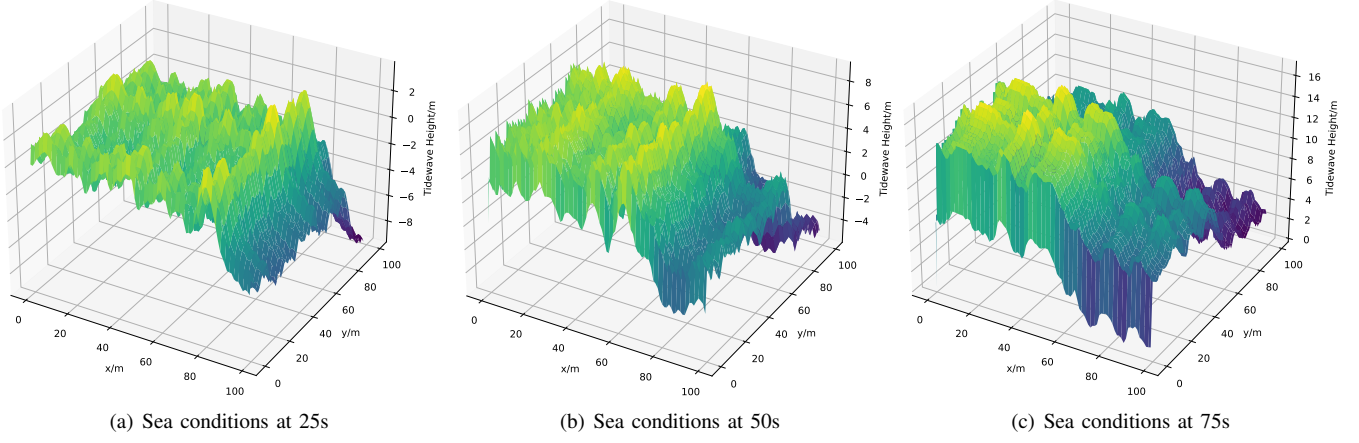


Fig. 3. The illustration of realistic extreme sea condition simulation via finite difference method at three different time points. (a) Sea conditions at 25s. (b) Sea conditions at 50s. (c) Sea conditions at 75s.

TABLE I
PARAMETERS OF THE ENVIRONMENT AND ALGORITHM

Parameters	Values
Experimental area	200m × 200m
USV sound level	135dB
USV transmit frequency	15kHz(AUV 1)/18kHz(AUV 2)
Hydrophone array d	0.033m
Water Depth	120m
Time step Δt	10s
Space step Δx	4m
Angular frequency ω	$2\pi/43200$ rad/s
Initial amplitude η_0	5m
Training episode	600
Steps in each episode	1000
Replay buffer size	$2 * 10^4$
Hidden layer size	128
Batch size	64
Policy update interval	2
Target policy noise	$\mathcal{N}(0, 0.1)$, clipped to ± 1.0
Discount factor γ	0.97
Actor learning rate	$1 * 10^{-3}$
Critic learning rate	$1 * 10^{-3}$
Soft update parameter	$1 * 10^{-3}$

- **Actor:** 3-layer MLP (128, 128, 128 units) with ReLU activations, outputting tanh-scaled actions.
- **Critics:** Twin 2-layer MLPs (128, 128 units) with ReLU activations.

The simulation experiments are conducted on a personal computer equipped with an AMD Ryzen 9 5950X processor and an NVIDIA GeForce RTX 4060 GPU, operating within a Python 3.8 virtual environment. Due to the adoption of an efficient computational approach for tidewave simulation, our code required approximately 3 hours to complete 600 episodes under the aforementioned configuration, demonstrating low computational resource demands. For other parameters, please refer to Table 1 for summary.

B. Realistic Extreme Sea Condition Simulation

The USV-AUV collaborative system's dual-domain operation (surface and subsurface) makes it particularly vulnerable

to marine disturbances. To address this, we employ two-dimensional tidal wave equations and ocean turbulence models to realistically simulate extreme sea conditions, accurately replicating disturbances that impact AUV positioning and performance for rigorous system validation. The simulation effects of sea conditions at three different time points (25s, 50s, 75s) have been shown in Fig. 3.

If we denote the wave velocity as $V_w = [u, v]$, and the gravitational acceleration as g , the water level η at coordinate point (x', y') can be calculated using Finite Difference Method (FDM). The equations' forward difference scheme using FDM can be listed as follows [37]:

$$\frac{u_{i,j}^{n+1} - u_{i,j}^n}{\Delta t} + g \frac{\eta_{i+1,j}^n - \eta_{i,j}^n}{\Delta x} = 0, \quad (19a)$$

$$\frac{v_{i,j}^{n+1} - v_{i,j}^n}{\Delta t} + g \frac{\eta_{i,j+1}^n - \eta_{i,j}^n}{\Delta y} = 0, \quad (19b)$$

$$\frac{\eta_{i,j}^{n+1} - \eta_{i,j}^n}{\Delta t} + \frac{(u \cdot h)_{i,j}^n - (u \cdot h)_{i-1,j}^n}{\Delta x} + \frac{(v \cdot h)_{i,j}^n - (v \cdot h)_{i,j-1}^n}{\Delta y} = 0, \quad (19c)$$

where $u_{i,j}^n$ and $v_{i,j}^n$ are the velocity components in x' and y' directions at grid point (i, j) and time step n , $\eta_{i,j}^n$ is the water level height, Δt is the time step, Δx and Δy are spatial steps, while h represents the water depth.

Moreover, considering the vortex center position, the turbulent velocity and vorticity can be numerically computed at grid point (i, j) through the ocean turbulence model's finite difference formulation [38]:

$$V_{x,i,j} = -\Gamma \cdot \frac{y_j - y_0}{2\pi [(x_i - x_0)^2 + (y_j - y_0)^2]} \left(1 - e^{-\frac{(x_i - x_0)^2 + (y_j - y_0)^2}{\delta^2}} \right), \quad (20a)$$

$$V_{y,i,j} = \Gamma \cdot \frac{x_i - x_0}{2\pi [(x_i - x_0)^2 + (y_j - y_0)^2]} \left(1 - e^{-\frac{(x_i - x_0)^2 + (y_j - y_0)^2}{\delta^2}} \right), \quad (20b)$$

$$\varpi_{i,j} = \frac{\Gamma}{\pi \delta^2} \cdot e^{-\frac{(x_i - x_0)^2 + (y_j - y_0)^2}{\delta^2}}, \quad (20c)$$

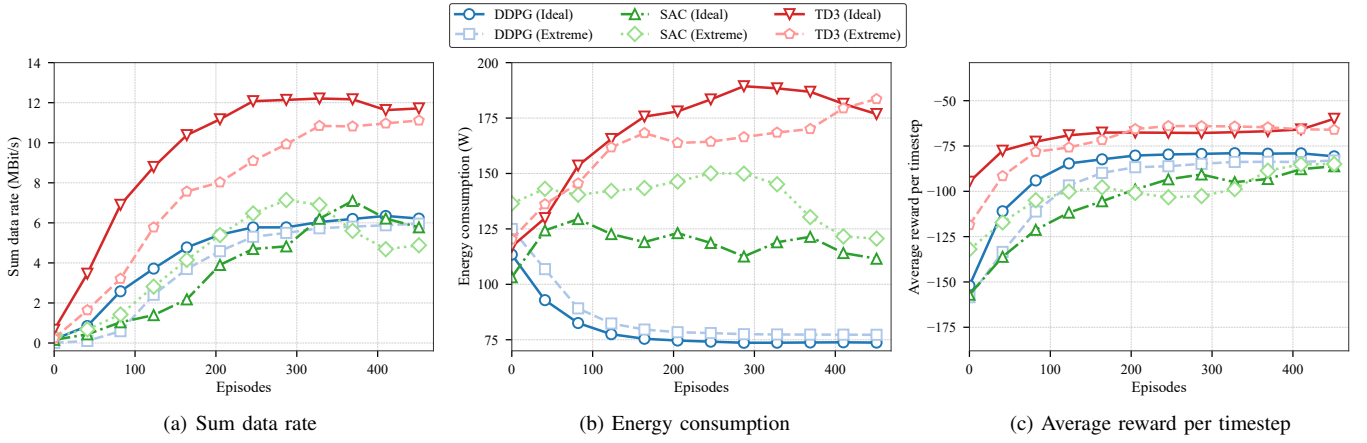


Fig. 4. The curves of sum data rate, energy consumption and average reward per timestep, using TD3, DDPG and SAC for RL training in ideal and extreme sea conditions, respectively. (a) Sum data rate. (b) Energy consumption. (c) Average reward per timestep.

TABLE II
COMPARISON OF DIFFERENT RL ALGORITHMS IN IDEAL AND EXTREME SEA CONDITIONS

	SDR	EC	ARPS	SSN
TD3 (ISC)	11.20±1.93	138.19±3.80	-60.69±7.81	47.0±5.52
TD3 (ESC)	10.78±1.70	147.81±5.09	-62.95±8.60	45.4±6.81
DDPG (ISC)	6.63±0.97	73.72±1.11	-80.70±6.94	30.8±3.97
DDPG (ESC)	6.35±1.57	77.23±0.89	-82.28±7.41	29.6±4.91
SAC (ISC)	5.97±2.66	111.57±13.23	-87.86±13.10	27.2±7.35
SAC (ESC)	5.58±2.35	117.76±17.30	-89.58±15.22	25.0±6.62
Baseline [5]	5.93±3.51	112.30±10.56	-87.95±12.08	25.8±7.94

where ϖ , δ , and Γ stand for the vorticity, radius, and intensity of the vortex, respectively.

C. State, Action Space and Reward Function Design

In this study, the full state vector of state $s_t^k \in \mathcal{S}$ for the k -th AUV at time t is composed of:

$$s_t^k = [\{\Delta \mathbf{p}_j^k\}_{j \neq k}, \Delta \mathbf{p}_{\text{target}}^k, \tilde{\mathbf{p}}_t^k, \rho_{\text{overflow}}, \mathbb{I}_{\text{border}}^k] \in \mathbb{R}^{6+2(m-1)}, \quad (21)$$

where $\{\Delta \mathbf{p}_j^k\}_{j \neq k} = \frac{\mathbf{p}_t^j - \mathbf{p}_t^k}{\|\mathbf{b}\|}$ denotes relative positions of other AUVs, with $\mathbf{p}_t^k \in \mathbb{R}^2$ denoting the 2D position of the k -th AUV, and $\mathbf{b} = [X_{\text{max}}, Y_{\text{max}}]^\top$ defining the environment boundaries. Besides, $\Delta \mathbf{p}_{\text{target}}^k = \frac{\mathbf{p}_{\text{target}}^k - \mathbf{p}_t^k}{\|\mathbf{b}\|}$ denotes the relative position to target SN, with $\mathbf{p}_{\text{target}}^k$ representing the position of the target SN assigned to the k -th AUV. Normalized self-position $\tilde{\mathbf{p}}_t^k = \frac{\mathbf{p}_t^k}{\|\mathbf{b}\|}$, while $\rho_{\text{overflow}} = \frac{N_{\text{DO}}}{N_{\text{POI}}}$ is the data overflow ratio. Additionally, $\mathbb{I}_{\text{border}}^k \in \{0, 1\}$ represents the border violation flag.

The full action vector of action $a_t^k \in \mathcal{A}$ for the k -th AUV is a 2D continuous vector:

$$a_t^k = [v_{\text{norm}}, \theta_{\text{norm}}]^\top, \quad v_{\text{norm}} \in [-1, 1], \quad \theta_{\text{norm}} \in [-1, 1], \quad (22)$$

where v_{norm} denotes expected normalized speed, which is linearly mapped to the physical range $[V_{\text{min}}, V_{\text{max}}]$: $v_{\text{norm}} = \frac{2(v_t^k - V_{\text{min}})}{V_{\text{max}} - V_{\text{min}}} - 1$. θ_{norm} stands for expected normalized direction, and is scaled to $[-\pi, \pi]$: $\theta_{\text{norm}} = \frac{\theta_t^k}{\pi}$.

Since reward is significant for RL training, we employ a shaped reward function that balances multiple objectives:

$$\mathcal{R} = \boldsymbol{\lambda}^T \mathbf{R} = \sum_{i=1}^p \lambda_i R_i, \quad (23)$$

where $\mathbf{R} = \{R_1, R_2, \dots, R_p\}$ represents distinct objectives. $\boldsymbol{\lambda} = \{\lambda_1, \lambda_2, \dots, \lambda_p\}$ control the relative weighting of these objectives. Substituting into underwater data collection task, our reward function is designed as follows:

$$\begin{aligned} \mathcal{R} = & -0.6d_k^{\text{target}} - 0.1\mathbb{I}_{\text{border}} - 0.05N_{\text{DO}} - \sum_{j \neq k} 6(12 - d_{kj}) \\ & + 12\mathbb{I}_{\text{TL}} - 0.085E_k, \end{aligned} \quad (24)$$

specifically, the terms d_k^{target} denotes AUV-SN distance, $\mathbb{I}_{\text{border}}$ represents border violation indicator, while N_{DO} stands for data overflow count. Besides, d_{kj} is inter-AUV distance, and \mathbb{I}_{TL} denotes transmission success flag, while E_k represents energy consumption.

D. Experiment Results and Analysis

To comprehensively assess the feasibility and effectiveness of our proposed system, we conducted a series of systematic experiments involving both training and evaluation phases. Initially, we implemented three state-of-the-art RL algorithms, TD3, DDPG and Soft Actor-Critic (SAC), to train two AUVs that were positioned by a USV. The training process was carried out under two distinct marine

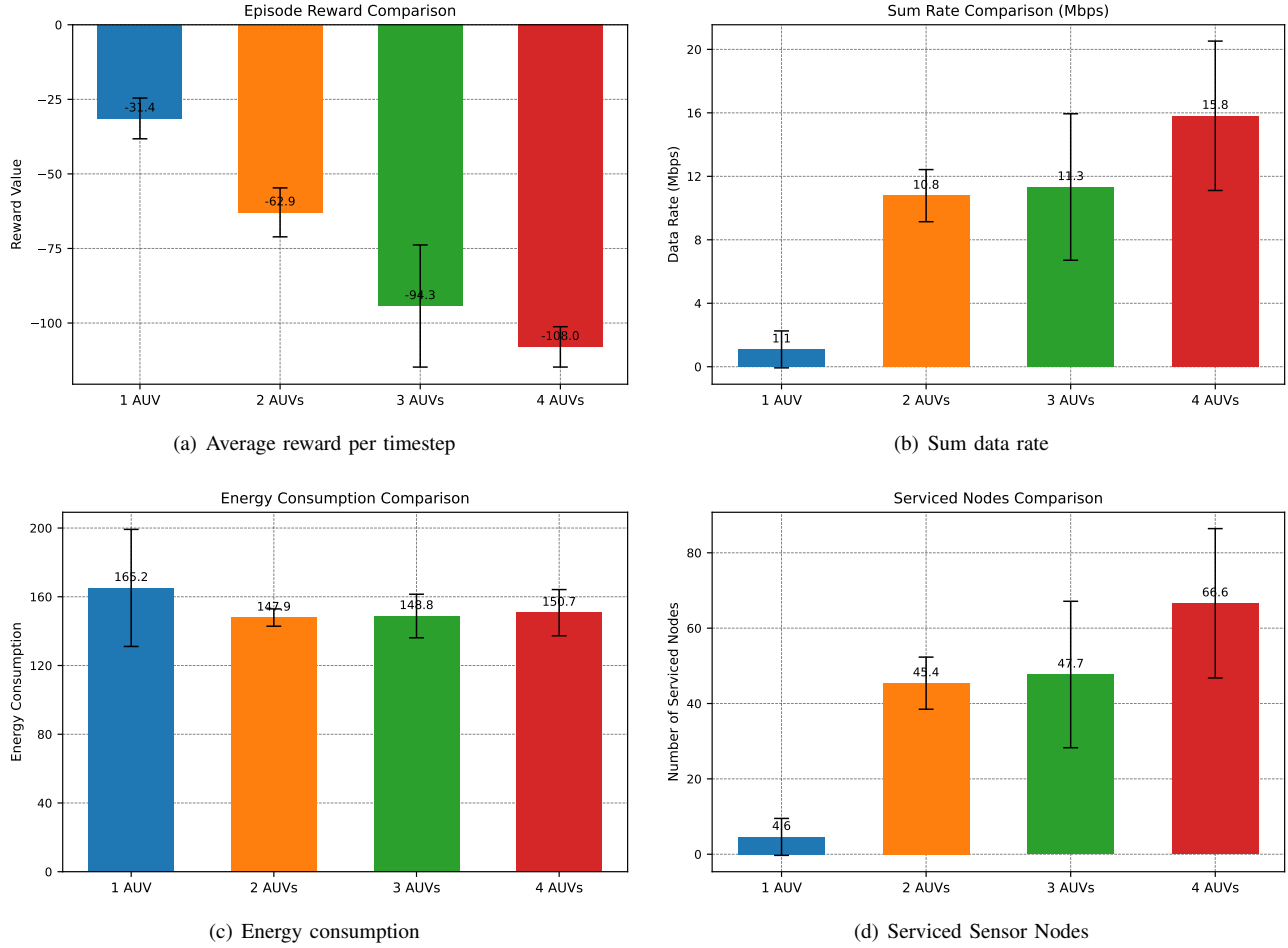


Fig. 5. The histogram of average reward per timestep, sum data rate, energy consumption and average reward per timestep, using RL to train 1 AUV, 2 AUVs, 3 AUVs and 4 AUVs in extreme sea conditions, respectively. (a) Average reward per timestep. (b) Sum data rate. (c) Energy consumption. (d) Serviced sensor nodes.

environments: ideal sea conditions and extreme sea conditions. As demonstrated in Fig. 4, the learning curves exhibit stable convergence and eventually reach performance levels comparable to expert policies, clearly indicating that the AUVs have successfully learned optimal navigation and data collection strategies through the RL training process. While we can also find that TD3 outperforms other algorithms and baseline in SDR and ARPT, although energy consumption is higher than others.

In addition, to further validate the system’s robustness, we conducted extensive environmental generalization tests comparing system performance between ideal and extreme sea conditions. The experimental results, summarized in Table 2 (where ISC and ESC represent Ideal Sea Conditions and Extreme Sea Conditions, while ARPS and SSN denote Average Reward Per Step and Serviced Sensor Nodes, respectively), reveal that despite the challenging environmental factors present in extreme conditions, the system maintains comparable performance metrics to those achieved in ideal conditions. This remarkable consistency in performance across different environmental scenarios strongly demonstrates the system’s exceptional robustness and adaptability

when operating in extreme sea conditions.

To further validate the scalability of the proposed USV-AUV collaboration framework, we conducted a new set of experiments using 1 AUV, 2 AUVs, 3 AUVs and 4 AUVs for underwater data collection tasks, evaluating their performance in extreme sea conditions, respectively. The results were plotted in the form of a histogram in Fig. 5. From the histogram we can obtain that as the number of AUVs increases, although ARPT shows a downward trend, the system’s SDR improves significantly. Specifically, when the number of AUVs increases from 1 to 4, the SDR and SSN increases by approximately 14.7 and 62, respectively. This indicates that multi-AUV collaboration can effectively distribute task loads and significantly enhance overall efficiency through parallel data collection. Although the increase in the number of AUVs also leads to higher EC, the growth remains within a reasonable range. For example, the EC for 4 AUVs is only about 1% higher than that for 3 AUVs and even 10% lower for a single AUV, which is far below the proportional improvement in SDR. This demonstrates the efficiency of the proposed system in optimizing resource allocation and path planning, ensuring performance gains while keeping

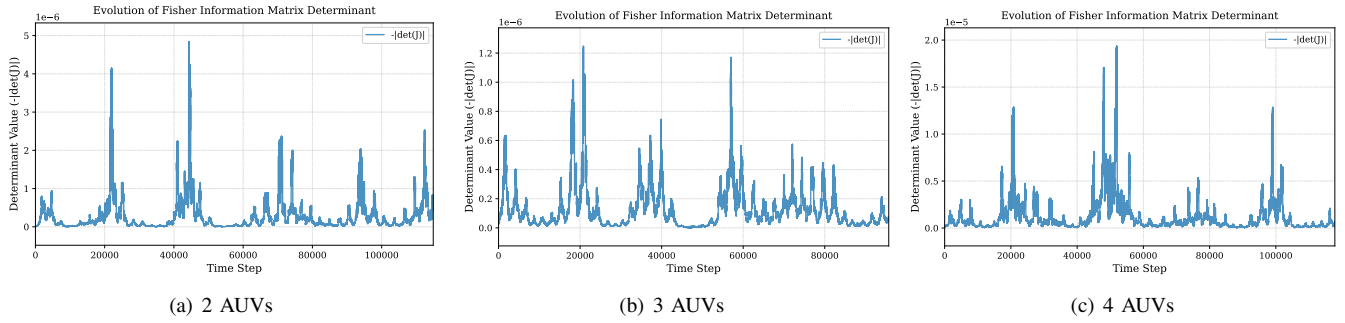


Fig. 6. Negative determinant value evolution of FIM in an operational episode using different number of AUVs. (a) 2 AUVs. (b) 3 AUVs. (c) 4 AUVs.

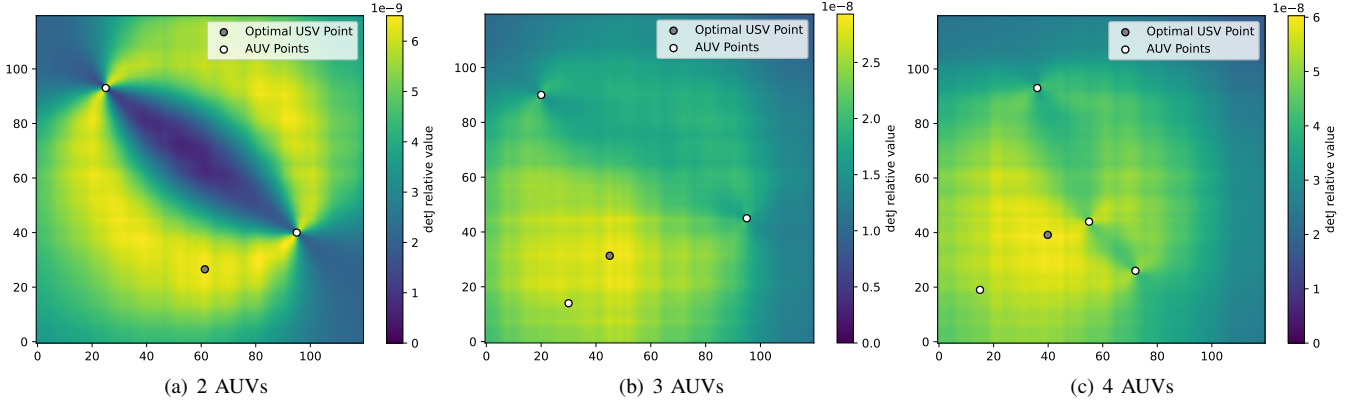


Fig. 7. The illustrations of the USV-AUV coordinate relationships in the collaborative system at some point. The optimal USV positions were determined through real-time optimization of FIM determinant value to minimize AUV positioning errors. (a) 2 AUVs: The optimal USV position is at coordinates [61.3, 26.5]. (b) 3 AUVs: The optimal USV position is at coordinates [45.2, 31.1]. (c) 4 AUVs: The optimal USV position is at coordinates [39.8, 39.2].

additional energy consumption at an acceptable level.

To further evaluate the robustness and scalability of the proposed USV-AUV collaborative system, we conducted additional experiments employing 2, 3, and 4 AUVs for underwater data collection tasks in extreme sea conditions. A key focus of these experiments was to minimize the negative determinant of the FIM in real-time during each operational episode, thereby optimizing USV path planning for enhanced AUV positioning accuracy. The results demonstrate that despite significant environmental disturbances (including ocean turbulence and strong waves), the system consistently maintained the FIM determinant’s negative value within a minimized range throughout each operational episode. As shown in Fig. 6, this achievement was observed across all tested configurations (2, 3, and 4 AUVs), with the minimization performance showing particular robustness in the extreme sea conditions. Furthermore, through visualization in Fig. 7, it was clearly observed that the USV’s path planning points consistently fell in the region with the lowest AUV positioning error. The optimal USV positions in the USV-AUV collaborative system were determined as follows:

- 2 AUVs configuration: Optimal USV position at [61.3, 26.5] for AUVs located at [25, 93] and [95, 40].
- 3 AUVs configuration: Optimal position at [45.2, 31.1] for AUVs at [20, 90], [95, 45], and [30, 14].
- 4 AUVs configuration: Optimal position at [39.8, 39.2]

for AUVs at [36, 93], [55, 44], [15, 19], and [72, 26].

These findings demonstrate the system’s capability to dynamically adapt the USV’s position in response to real-time AUV localization requirements. Notably, when the USV positioned itself at the point of minimized FIM determinant negative value, we observed a significant reduction in AUV positioning errors. This empirical evidence strongly supports the fundamental importance of FIM optimization in effective path planning for our proposed USV-AUV collaborative system.

In addition to the base experiments, we leveraged the expert policy trained using the TD3 algorithm to coordinate a multi-AUV system executing the underwater data collection task in extreme sea conditions. Fig. 8 illustrates the complete trajectories of both the AUVs and the USV during a representative RL training episode, showcasing their coordinated movement patterns and task execution strategies. To quantitatively evaluate the advantages of our USV-AUV collaborative framework, we conducted a detailed analysis of the positioning accuracy under three distinct operational scenarios:

- Employing USV path planning through FIM optimization techniques.
- Maintaining the USV at a fixed position at original coordinates (0,0).
- Maintaining the USV at a fixed position at midpoint

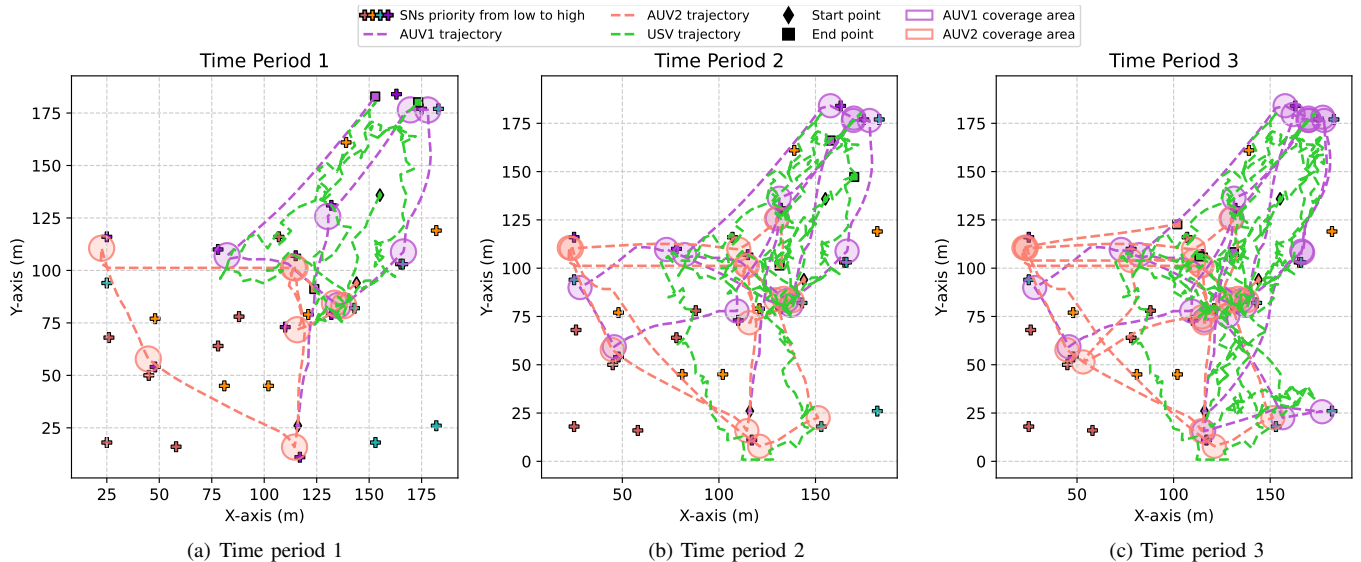


Fig. 8. Trajectories of AUVs and USV in three different time periods of an operational episode. (a) Time period 1. (b) Time period 2. (c) Time period 3.

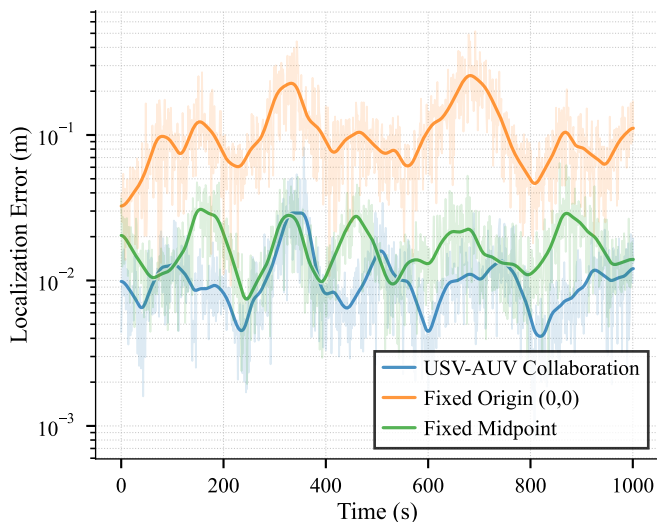


Fig. 9. Positioning error of the AUV with USV fixed at (0,0) and (100, 100), and path planning using FIM optimization, respectively.

coordinates (100,100).

The positioning error comparison presented in Fig. 9 clearly demonstrates that the FIM-optimized USV path planning approach achieves significantly lower positioning errors compared to the fixed-position alternatives. These results provide compelling evidence for the superior performance of USBL positioning when combined with optimized USV path planning, even when operating under the most challenging sea conditions. The system’s ability to maintain high positioning accuracy in such environments further confirms its practical applicability for real-world underwater operations.

V. CONCLUSION

In this study, we developed a USV–AUV collaborative system to enhance the performance of underwater tasks in extreme sea conditions, which consists of two key components:

(1) high-precision multi-AUV localization achieved through USV path planning via FIM optimization, and (2) RL-based multi-AUV cooperative task execution. Comprehensive experiments in the underwater data collection task validated the system’s feasibility and superior performance, while demonstrating effective USV-AUV coordination and robust operation in extreme sea conditions. To support further research in this field, we have open-sourced a simulation code demo at: <https://github.com/360ZMEM/USV-AUV-colab>.

In the future, we aim to explore online learning and adaptive techniques to enable real-world deployment with real-time environmental adaptation for the USV-AUV system in extreme sea conditions. Our goal is to address practical challenges such as the Sim2Real gap observed in real-world applications.

REFERENCES

- [1] J. Rutledge, W. Yuan, J. Wu, S. Freed, A. Lewis, Z. Wood, T. Gambin, and C. Clark, “Intelligent shipwreck search using autonomous underwater vehicles,” in *2018 IEEE International Conference on Robotics and Automation (ICRA)*, 2018, pp. 6175–6182.
- [2] L. Hawkes, O. Exeter, S. Henderson, C. Kerry, A. Kukulya, J. Rudd, S. Whelan, N. Yoder, and M. Witt, “Autonomous underwater videography and tracking of basking sharks,” *Animal Biotelemetry*, vol. 8, 08 2020.
- [3] F. L. Peña, F. Orjales, and A. Deibe, “Development of a collaborative host-guest unmanned underwater vehicle docking system for inspection and maintenance of offshore structures,” in *OCEANS 2023 - MTS/IEEE U.S. Gulf Coast*, 2023, pp. 1–5.
- [4] J. Du, B. Jiang, C. Jiang, Y. Shi, and Z. Han, “Gradient and channel aware dynamic scheduling for over-the-air computation in federated edge learning systems,” *IEEE Journal on Selected Areas in Communications*, vol. 41, no. 4, pp. 1035–1050, 2023.
- [5] Z. Zhang, J. Xu, G. Xie, J. Wang, Z. Han, and Y. Ren, “Environment- and energy-aware auv-assisted data collection for the internet of underwater things,” *IEEE Internet of Things Journal*, vol. 11, no. 15, pp. 26 406–26 418, 2024.
- [6] L. Zhang, C. Tang, P. Chen, and Y. Zhang, “Gaussian parameterized information aided distributed cooperative underwater positioning algorithm,” *IEEE Access*, vol. 8, pp. 64 634–64 645, 2020.

- [7] A. Bahr, J. J. Leonard, and A. Martinoli, "Dynamic positioning of beacon vehicles for cooperative underwater navigation," in *2012 IEEE/RSJ International Conference on Intelligent Robots and Systems*, 2012, pp. 3760–3767.
- [8] A. Vasilijevic, D. Nad, and N. Miskovic, "Autonomous surface vehicles as positioning and communications satellites for the marine operational environment — step toward internet of underwater things," in *2018 IEEE 8th International Conference on Underwater System Technology: Theory and Applications (USYS)*, 2018, pp. 1–5.
- [9] B. R. Page and N. Mahmoudian, "Auv docking and recovery with usv: An experimental study," in *OCEANS 2019 - Marseille*, 2019, pp. 1–5.
- [10] L.-F. Wu, M. Rastgaar, and N. Mahmoudian, "Heterogeneous multi-robot (uav-usv-auv) collaborative exploration with energy replenishment," *IFAC-PapersOnLine*, vol. 58, no. 20, pp. 159–164, 2024, 15th IFAC Conference on Control Applications in Marine Systems, Robotics and Vehicles CAMS 2024. [Online]. Available: <https://www.sciencedirect.com/science/article/pii/S2405896324018020>
- [11] Y. Girdhar, N. McGuire, L. Cai, S. Jamieson, S. McCammon, B. Claus, J. E. S. Soucie, J. E. Todd, and T. A. Mooney, "Curee: A curious underwater robot for ecosystem exploration," in *2023 IEEE International Conference on Robotics and Automation (ICRA)*, 2023, pp. 11 411–11 417.
- [12] Z. Fang, J. Wang, J. Du, X. Hou, Y. Ren, and Z. Han, "Stochastic optimization-aided energy-efficient information collection in internet of underwater things networks," *IEEE Internet of Things Journal*, vol. 9, no. 3, pp. 1775–1789, 2022.
- [13] J. Xu, G. Xie, X. Wang, Y. Ding, and S. Zhang, "Usv-auv collaboration framework for underwater tasks under extreme sea conditions," in *ICASSP 2025 - 2025 IEEE International Conference on Acoustics, Speech and Signal Processing (ICASSP)*, 2025, pp. 1–5.
- [14] Z. Wang, J. Xu, Y. Feng, Y. Wang, G. Xie, X. Hou, W. Men, and Y. Ren, "Fisher-information-matrix-based usbl cooperative location in usv-auv networks," *Sensors*, vol. 23, no. 17, 2023. [Online]. Available: <https://www.mdpi.com/1424-8220/23/17/7429>
- [15] P. Jiang, S. Song, and G. Huang, "Attention-based meta-reinforcement learning for tracking control of auv with time-varying dynamics," *IEEE Transactions on Neural Networks and Learning Systems*, vol. 33, no. 11, pp. 6388–6401, 2022.
- [16] X. Lin, N. Karapetyan, K. Joshi, T. Liu, N. Chopra, M. Yu, P. Tokekar, and Y. Aloimonos, "Uivnav: Underwater information-driven vision-based navigation via imitation learning," in *2024 IEEE International Conference on Robotics and Automation (ICRA)*, 2024, pp. 5250–5256.
- [17] Z. Xia, J. Du, J. Wang, C. Jiang, Y. Ren, G. Li, and Z. Han, "Multi-agent reinforcement learning aided intelligent uav swarm for target tracking," *IEEE Transactions on Vehicular Technology*, vol. 71, no. 1, pp. 931–945, 2022.
- [18] L. Paull, S. Saeedi, M. Seto, and H. Li, "Auv navigation and localization: A review," *IEEE Journal of Oceanic Engineering*, vol. 39, no. 1, pp. 131–149, 2014.
- [19] E. I. Sarda and M. R. Dhanak, "A usv-based automated launch and recovery system for auvs," *IEEE Journal of Oceanic Engineering*, vol. 42, no. 1, pp. 37–55, 2017.
- [20] B. Zhang, D. Ji, S. Liu, X. Zhu, and W. Xu, "Autonomous underwater vehicle navigation: A review," *Ocean Engineering*, vol. 273, p. 113861, 2023. [Online]. Available: <https://www.sciencedirect.com/science/article/pii/S0029801823002457>
- [21] T. Matsuda, T. Maki, and M. Sangekar, "Intelligent seafloor survey by cooperative multiple auvs based on real-time analysis of a bathymetry map," in *OCEANS 2017 - Anchorage*, 2017, pp. 1–5.
- [22] L. J. Johnson, R. J. Green, and M. S. Leeson, "Hybrid underwater optical/acoustic link design," in *2014 16th International Conference on Transparent Optical Networks (ICTON)*, 2014, pp. 1–4.
- [23] Z. Yang, J. Du, Z. Xia, C. Jiang, A. Benslimane, and Y. Ren, "Secure and cooperative target tracking via auv swarm: A reinforcement learning approach," in *2021 IEEE Global Communications Conference (GLOBECOM)*, 2021, pp. 1–6.
- [24] S. Wirtensohn, H. Wenzl, T. Tietz, and J. Reuter, "Parameter identification and validation analysis for a small usv," in *2015 20th International Conference on Methods and Models in Automation and Robotics (MMAR)*, 2015, pp. 701–706.
- [25] A. D. Wilson, J. A. Schultz, and T. D. Murphey, "Trajectory synthesis for fisher information maximization," *IEEE Transactions on Robotics*, vol. 30, no. 6, pp. 1358–1370, 2014.
- [26] B. Porat, "On the fisher information for the mean of a gaussian process," *IEEE Transactions on Signal Processing*, vol. 43, no. 8, pp. 2033–2035, 1995.
- [27] J. Gong, B. Zou, C. Xu, J. Xu, and X. You, "Hybrid learning based on fisher linear discriminant," *Information Sciences*, vol. 667, p. 120465, 2024. [Online]. Available: <https://www.sciencedirect.com/science/article/pii/S0020025524003785>
- [28] G. Han, A. Gong, H. Wang, M. Martínez-García, and Y. Peng, "Multi-auv collaborative data collection algorithm based on q-learning in underwater acoustic sensor networks," *IEEE Transactions on Vehicular Technology*, vol. 70, no. 9, pp. 9294–9305, 2021.
- [29] Y. Sun, X. Ran, G. Zhang, X. Wang, and H. Xu, "Auv path following controlled by modified deep deterministic policy gradient," *Ocean Engineering*, vol. 210, p. 107360, 2020. [Online]. Available: <https://www.sciencedirect.com/science/article/pii/S0029801820303917>
- [30] I. Carlucho, M. De Paula, S. Wang, B. V. Menna, Y. R. Petillot, and G. G. Acosta, "Auv position tracking control using end-to-end deep reinforcement learning," in *OCEANS 2018 MTS/IEEE Charleston*, 2018, pp. 1–8.
- [31] Y. Li, W. Yu, H. Xu, and X. Guan, "Robust multiple autonomous underwater vehicle cooperative localization based on the principle of maximum entropy," *IEEE Transactions on Automation Science and Engineering*, pp. 1–1, 2025.
- [32] D. Wang, Y. Shen, J. Wan, Q. Sha, G. Li, G. Chen, and B. He, "Sliding mode heading control for auv based on continuous hybrid model-free and model-based reinforcement learning," *Applied Ocean Research*, vol. 118, p. 102960, 2022. [Online]. Available: <https://www.sciencedirect.com/science/article/pii/S0141118721004247>
- [33] P. Jiang, S. Song, and G. Huang, "Attention-based meta-reinforcement learning for tracking control of auv with time-varying dynamics," *IEEE Transactions on Neural Networks and Learning Systems*, vol. 33, no. 11, pp. 6388–6401, 2022.
- [34] H. Lee, K. Kim, T. Chung, and H. Ko, "Deep learning-based ultra short baseline underwater positioning," in *2023 International Conference on Artificial Intelligence in Information and Communication (ICAIC)*, 2023, pp. 856–859.
- [35] L. Meng and J. C. Spall, "Efficient computation of the fisher information matrix in the em algorithm," in *2017 51st Annual Conference on Information Sciences and Systems (CISS)*, 2017, pp. 1–6.
- [36] S. Fujimoto, H. van Hoof, and D. Meger, "Addressing function approximation error in actor-critic methods," in *Proceedings of the 35th International Conference on Machine Learning*, ser. Proceedings of Machine Learning Research, J. Dy and A. Krause, Eds., vol. 80. PMLR, 10–15 Jul 2018, pp. 1587–1596. [Online]. Available: <https://proceedings.mlr.press/v80/fujimoto18a.html>
- [37] Z. li Wang and Y. fen Geng, "Two-dimensional shallow water equations with porosity and their numerical scheme on unstructured grids," *Water Science and Engineering*, vol. 6, no. 1, pp. 91–105, 2013. [Online]. Available: <https://www.sciencedirect.com/science/article/pii/S1674237015302271>
- [38] Z. Fang, J. Wang, J. Du, X. Hou, Y. Ren, and Z. Han, "Stochastic optimization-aided energy-efficient information collection in internet of underwater things networks," *IEEE Internet of Things Journal*, vol. 9, no. 3, pp. 1775–1789, 2022.